



Seismic performance and impact of geometric nonlinearity on 3D steel braced frame building models

Hamid Foroughi¹, Gengrui Wei², Shahabeddin Torabian³, Matthew R. Eatherton⁴, Benjamin W. Schafer⁵

Abstract

The objective of this paper is to examine the seismic performance of steel braced frame buildings, braced by either buckling restrained braces (BRBs) or concentrically braced frames (CBFs). A unique feature of the investigation is the creation of fully three-dimensional building models so that the interaction of the building diaphragm with the vertical lateral force resisting systems can be examined in detail. Few investigations of seismic performance have explored this interaction as models are typically two-dimensional. The work is conducted as a portion of the ongoing Steel Diaphragm Innovation Initiative – and is of particular interest in better understanding the design and performance of building diaphragms. Another novel aspect of the modeling is a specific look at the impact of including or ignoring geometric nonlinearity (e.g., P- Δ and P- δ) in the building models. There are questions about the impact of geometric nonlinearity and its application both in equivalent lateral force designs and in nonlinear time history analysis. The building models are used as case studies to explicitly demonstrate the impact of geometric nonlinearity on overall building response. The building simulation studies are conducted in OpenSees and are currently ongoing. Completed work reported herein includes analysis of building archetypes designed to the current U.S. seismic standards and potential diaphragm design alternatives for a 1 and 4-story BRB and CBF steel frames. The results demonstrate the sensitivity of building diaphragm demands to the vertical lateral force resisting system and to the inclusion of geometric nonlinearity in the building response.

1. Introduction

Seismic performance of buildings depends on both the vertical lateral force resisting system (LFRS), such as braced frames, and the horizontal LFRS, such as the roof or floor diaphragm. Conventional seismic design of buildings assumes that the vertical LFRS, e.g. a concentrically brace frame (CBF) or buckling restrained braces (BRB), is the only source of inelastic action and hysteretic energy dissipation in the structure. However, it has been shown that diaphragms

¹ Graduate Research Assistant, Johns Hopkins University, <hforoug1@jhu.edu>

² Graduate Research Assistant, Virginia Tech, <gwei1@vt.edu>

³ Associate Research Scientist, Johns Hopkins University, <torabian@jhu.edu >

⁴ Associate Professor, Virginia Tech, <meather@vt.edu >

⁵ Professor, Johns Hopkins University, <schafer@jhu.edu>

designed using traditional design procedures may be subject to inelasticity even during design level earthquakes (Rodriguez et al. 2007), and in the extreme may experience collapse such as happened for several concrete parking garages with precast concrete diaphragms during the 1994 Northridge earthquake (EERI 1996). The role of the diaphragm in energy dissipation may be particularly pronounced for single-story structures when the story stiffness is far greater than the in-plane diaphragm stiffness – a condition that can happen in steel buildings with braced frames and bare steel deck roof diaphragms.

Today in U.S. seismic design provisions, i.e. ASCE 7-16 (ASCE 2010), two different design methodologies exist for the seismic design of diaphragms. Traditional diaphragm design procedures assume the diaphragm demands are reduced by the response modification factor, R , which is associated with the vertical system alone. While, in the new alternative diaphragm design procedures, currently only applicable to concrete and wood diaphragms, a diaphragm response modification factor, R_s , is employed to reduce (or increase) the diaphragm demands based on the ductility and overstrength of the diaphragm alone. Today, there is no agreed upon R_s factor for bare steel deck or steel deck with concrete filled diaphragms.

Equivalent lateral force (ELF) based design in ASCE 7-16, irrespective of the diaphragm design details, does not emphasize the impact of geometric nonlinearity in assessment of the building – and is not well aligned with modern frame stability methods such as the Direct Analysis Method promoted in U.S. steel standards (AISC 360-16). Thus, two important questions related to the seismic performance of steel frames are (a) what is the impact of changes in the diaphragm design on the building response, and (b) what is the impact of geometric nonlinearity on the building response? In this paper these two questions are explored through the design of BRB and CBF building archetypes with various diaphragm design options and analysis of the building archetypes with and without geometric nonlinearity. Nonlinear static pushover analyses and response history analyses using 44 ground motions scaled to two hazard levels are performed to study the behavior and seismic performance of the buildings.

2. Design and Modeling of Steel Building Archetypes

A series of detailed three-dimensional building archetypes have been developed for the Steel Diaphragm Innovation Initiative (SDII) as reported in Torabian et al. (2017). Here a subset of these buildings are selected for detailed study. First the basic building design parameters are summarized, followed by a discussion of the modeling strategies incorporated in the simulations conducted.

2.1 Archetype Design

To develop the archetype building designs one-story and four-story steel braced-frame buildings are designed using current U.S. design provisions: ASCE 7-16, AISC 341-16, AISC 360-16 and analyzed in SAP2000. Fig. 1 provides the basic building plan with dimensions of 91.5 meters (300 feet) by 30.5 meters (100 feet) and a story height of 4.27 meters (12.5 feet). The building has four bays braced with BRBs or hollow structural section CBFs in each orthogonal direction. Bare steel deck was detailed for the roof based on loads of to 2.06 KN/m^2 (42 psf) dead load and 0.96 KN/m^2 (20 psf) live load, and steel deck with concrete-filled diaphragms are employed for the floors with 4.07 KN/m^2 (85 psf) dead load and 2.06 KN/m^2 (50 psf) live load. The archetype buildings are assumed to be located in an arbitrary site in Irvine, California, with risk category II and site class

D. The design spectral accelerations at short periods and at a 1-second period are 1.030g and 0.569g, respectively. The diaphragm is designed following three different alternatives: (1) traditional ELF-based diaphragm demands as found in ASCE 7-10 or earlier and in the main body of ASCE7-16, and alternative diaphragm design with (2) $R_s=1.0$, or (3) $R_s=3.0$.

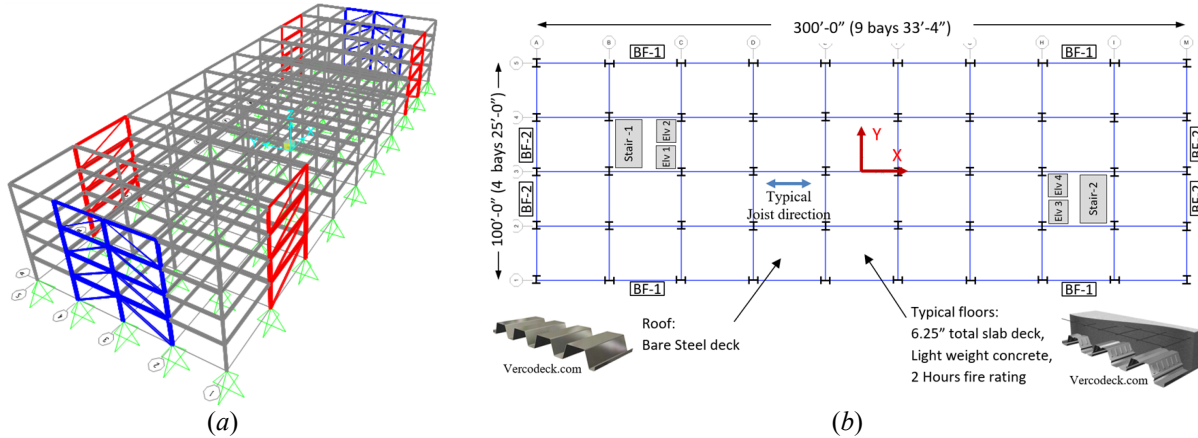


Figure 1: Schematic view of four-story archetype building: (a) 3D model, (b) typical plan

For the one-story CBF archetype building, the diaphragm design force is 39.55 KN/m (2.71 $kips/ft$) in the short direction of the building (weak direction of the diaphragm) for both traditional design forces from Section 12.10.1 of ASCE 7-16 or the alternative diaphragm design provisions ($R_s=3.0$). In both cases the minimum allowed diaphragm design force governs. For the four-story BRB archetype building Table 1 provides the baseline diaphragm force demands and demonstrates that they are again the same for traditional diaphragm design and the alternative diaphragm design provisions with $R_s = 3$. Further details of the archetype buildings and the design process can be found in (Torabian et al. 2017).

Table 1: Four-story BRB Archetype Diaphragm Design Forces for Different Design Procedures (per unit length along short direction of building, in kN/m)

| Archetype Building | Level | Diaphragm Design Procedure | |
|--------------------|-----------------------|----------------------------|-------------------------|
| | | Traditional | $R_s = 3.0$ |
| four-story | Roof | 19.11 (1.31 $kips/ft$) | 19.11(1.31 $kips/ft$) |
| | 4 th Level | 38.26 (2.21 $kips/ft$) | 38.26 (2.21 $kips/ft$) |
| | 3 rd Level | 38.26 (2.21 $kips/ft$) | 38.26 (2.21 $kips/ft$) |
| | 2 nd Level | 38.26 (2.21 $kips/ft$) | 38.26 (2.21 $kips/ft$) |

2.2 Archetype Simulation

A computational model of the archetype buildings was created in the software, *OpenSees*, with nonlinear phenomenological elements for the diaphragm and CBF and BRB braces as detailed in subsequent sections. All columns are pinned at their base. All beam-to-column and beam-to-beam joints are pinned with the exception of the braced bays which use semirigid connections at the beam-to-column joint to simulate the influences of the gusset plates. As recommended by FEMA P695 the gravity loads include a combination of dead and live loads (1.05D+0.25L). Mass was determined from the dead loads and lumped at the column nodes on each floor. For nonlinear response history analysis, Rayleigh damping with a critical damping ratio equal to 2% for the 1st and 2nd mode is used for the archetype building models. Both material and geometric nonlinearity are considered in the analysis, except where otherwise designated in the model results.

The two key nonlinear building components examined herein are the diaphragm and the concentric braces in the frames. These two elements are calibrated using existing data and then appropriately modified for use in the archetype building. Calibration and the modeling details for these building elements are provided in the following two sections

2.3 Diaphragm Modeling

The archetype building designs employ both bare steel deck and steel deck with concrete-filled diaphragms. Existing experiments are used to calibrate accurate nonlinear hysteretic models for the in-plane diaphragm response. The SDII cantilever diaphragm test database was utilized to select appropriate test specimens (O'Brien et al. 2017). For a typical bare steel deck roof diaphragm Specimen 33 with 20-gage 38.1 mm (1.5 in). deep B-deck and employing PAFs for the structural connectors and screws for the sidelap connections, based on testing of Martin (2002) was found to have sufficient design strength to match the roof demands for the baseline archetype building, herein denoted as SP1. For a typical steel deck with concrete fill test specimen 3/6.25-4-L-NF-DT which consisted of 72.6 mm (3 in). deck, with lightweight concrete fill and 158.75 mm (6.25 in). total thickness from Lowes and Altoontash (2003), herein denoted as SP2 was selected.

The test results are reported from cantilever diaphragm tests as depicted in Fig. 2a. The in-plane response is simulated through nonlinear truss elements as depicted in Fig. 2b. The Pinching4 material model in OpenSees is used for the truss elements to simulate the hysteretic behavior and capture cyclic strength and stiffness degradation behavior of the diaphragms. The parameters of the Pinching4 model are fit to the selected test results employing a multi-level optimization procedure with independent objective functions including cumulative strain energy, peak load, and degradation slopes. Table 2 provides the final calibrated Pinching 4 material parameters including backbone stresses and strains and cyclic strength and stiffness degradation for the two selected diaphragm specimens. A comparison of the hysteretic response from the calibrated diaphragm simulation and that from the experiment is shown in Fig. 2. The dimensions of the archetype building diaphragm units do not directly coincide with those of the test specimens, therefore the strategy described in Qayyum (2017) is adopted to modify the backbone parameters so that the diaphragm shear strength per unit length is consistently represented.

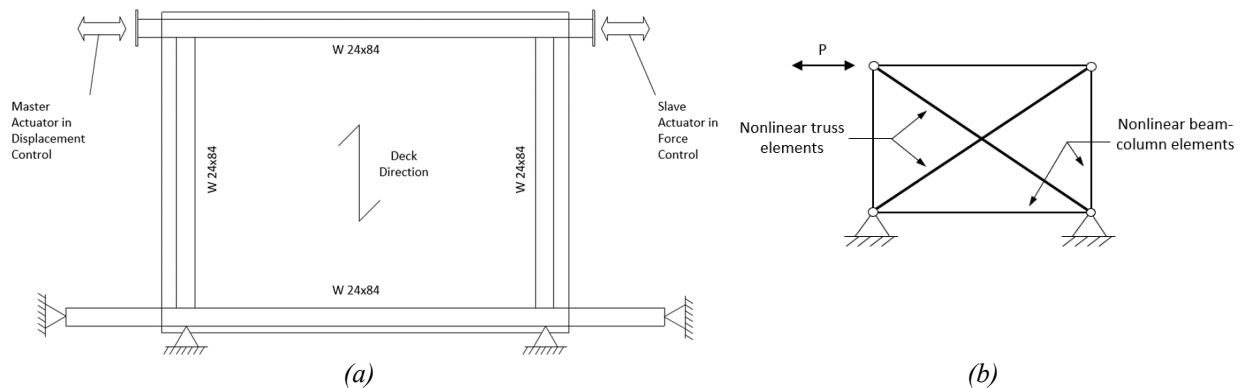


Figure 2: Cantilever diaphragm test: (a) schematic view of SP2 test setup, (b) computational model

Table 2: Calibrated Pinching4 Material Model Parameters

| Test | Backbone | | | | Pinching | | | Strength Degradation | | | | | Stiffness Degradation | | | | Energy Dissipation | |
|------|------------------------------------|------------------------------------|------------------------------------|------------------------------------|----------------------------------|------------------------|----------------------------------|----------------------|--------|--------|--------|------------|-----------------------|------------------|------------------|------------------|--------------------------|------|
| | ε_1, σ_1 (MPa) | ε_2, σ_2 (MPa) | ε_3, σ_3 (MPa) | ε_4, σ_4 (MPa) | r_{Δ^+} r_{Δ^-} | r_{p^+} r_{p^-} | u_{Δ^+} u_{Δ^-} | gF_1 | gF_2 | gF_3 | gF_4 | gF_{lim} | gK_1 gD_1 | gK_2 gD_2 | gK_3 gD_3 | gK_4 gD_4 | gK_{lim} gD_{lim} | gE |
| SP1 | 0.0008, 152.9 (22.18 ksi) | 0.0017, 199.2 (28.89 ksi) | 0.0033, 211.6 (30.69 ksi) | 0.0053, 165.3 (23.97 ksi) | 0.20, 0.35 | 0.20, 0.35 | 0.10, 0.12 | 0 | 0.35 | 0 | 0.70 | 0.90 | 0, 0 | 0, 0.50 | 0, 0 | 0, 0.75 | 0, 0.90 | 4.31 |
| SP2 | 0.0005, 437.6 (63.46 ksi) | 0.0006, 526.8 (76.41 ksi) | 0.0014, 740.5 (107.4 ksi) | 0.014, 333.2 (48.33 ksi) | -0.06, -0.06 | 0.12, 0.12 | 0.11, 0.11 | 0 | 0.83 | 0.0 | 0.46 | 0.33 | 1.09, 0.14 | 0.76, 0.47 | 0.32, 0.12 | 0.75, 0.10 | 1.04, 0.61 | 4.29 |

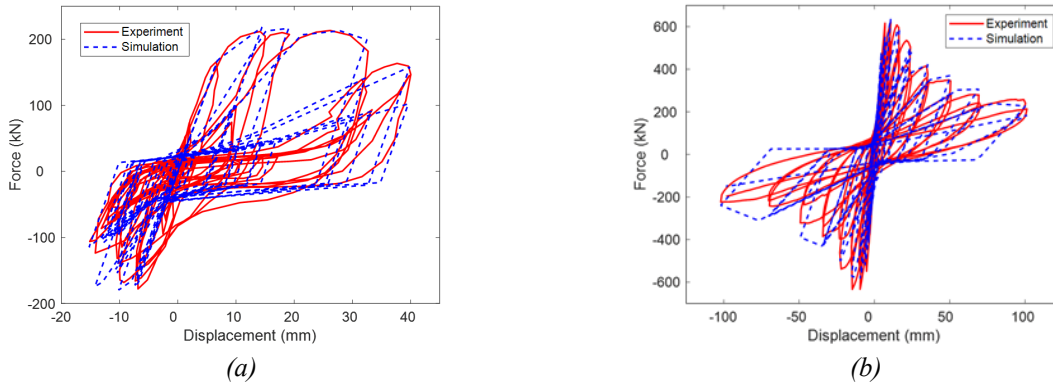


Figure 3: Hysteretic response of diaphragm from experiment and simulation: (a) SP1, (b) SP2

2.4 Brace Modeling

Two types of concentric braces are considered in the building archetypes studied herein: BRBs and hollow HSS sections. The modeling approaches adapted for these key building components are discussed in the following.

The BRB model focuses on the response of the restrained, yielding, core. As shown in Fig. 4a, the BRB core is represented by a nonlinear truss element with Steel02 material model in *OpenSees*. The non-yielding segments on both ends of the brace are modeled with elastic beam-column elements, and another elastic beam-column element with negligible cross-section area and large bending stiffness is also used to connect the non-yielding segments to fix the rotational degrees of freedom and prevent instability of the truss element. The calibration of the BRB core material model was conducted by Eatherton et al. (2014) to match the behavior of a specimen tested by Fahnestock et al. (2007) and the same material model is used in this study. Fig. 4b provides the hysteretic curves of the calibrated model as compared to the selected test results.

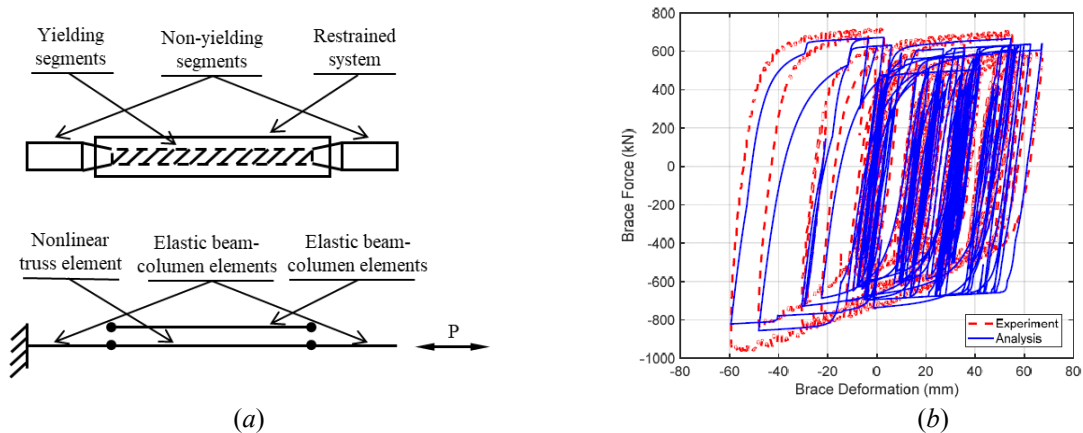


Figure 4: BRB computational model: (a) configuration of a typical BRB and the computational model, (b) hysteretic curves for calibration (adapted from Eatherton et al. (2014))

Traditional hollow structural section concentric braces are prone to buckle when they are under compression. To simulate the CBF behavior in both tension and compression, a computational *OpenSees* model is developed which is calibrated against experimental results. Experimental studies from Popov and Black (1981), Fell (2009), and Han (2007) are selected. The *OpenSees Steel02* material model as a fiber section is used to simulate the material nonlinear behavior of a single brace under cyclic load. A hollow structural section with pinned boundary conditions is used in the computational model. Geometric nonlinearity must be included in the analysis so that buckling in compression will occur (either co-rotational or p-delta in the *OpenSees* formulation). To insure accurate buckling response an out-of-straightness geometric imperfection of $L/1000$ is included in the middle of the brace, and the brace is discretized into at least 10 elements along the length. The brace model is capable of capturing both the tension and compression response as shown in Fig. 5. The calibrated Steel02 material parameters are provide in Table 3. It is important to note that this model of the brace neglects explicit modeling of local buckling and does not capture fracture in the braces or connections thus drift limits on the braced frames must be monitored.

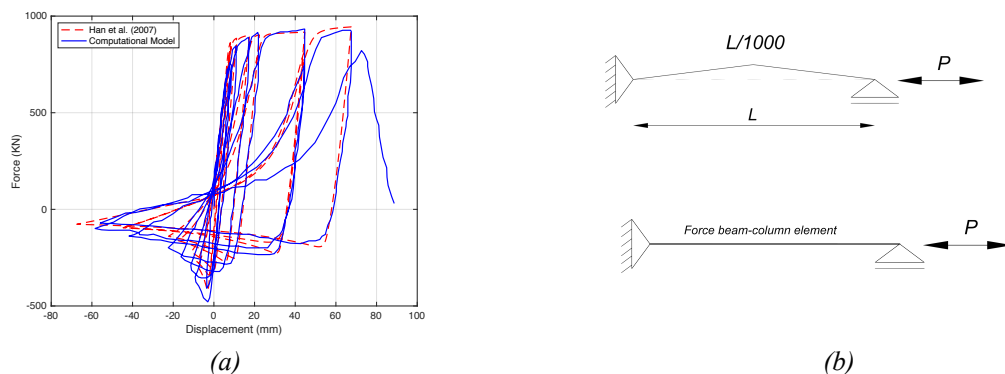


Figure 5: Concentric brace computational model: (a) Hysteretic response of CBF from experiment and simulation, Han (2007), (b) OpenSees model

Table 3: Steel02 material model parameters for three different experimental studies

| Experimental Study | F_y (MPa) | b | R_0 | CR_1 | CR_2 | a_1 | a_2 | a_3 | a_4 |
|--------------------|--------------|-------|-------|--------|--------|-------|-------|-------|-------|
| Popov and Black | 380 (55 ksi) | 0.002 | 20 | 0.925 | 0.15 | 0 | 1 | 0.1 | 5 |
| Fell et al. | 462 (67 ksi) | 0.002 | 20 | 0.925 | 0.15 | 0 | 1 | 0.1 | 5 |
| Han et al. | 414 (60 ksi) | 0.002 | 20 | 0.925 | 0.15 | 0 | 1 | 0.1 | 5 |

3 Geometric Nonlinearity in OpenSees

Today it is widely recognized that accurate structural analysis requires formulation of the equilibrium conditions in the deformed state. This reality invalidates traditional Lagrangian-based linear elasticity and results in complications for a building analysis. The complications are generally understood as deriving from two classes: material and geometric. Material nonlinearity influences the fundamental constitutive response and is typically handled at the element level. Geometric nonlinearity encompasses the nonlinearity derived from considering deformation alone – this may be at the constitutive level in terms of higher-order definitions of strain, or at the building level in terms of geometric transformations of the building joints (commonly referred to as P- Δ effects). A variety of potential formulations exist for including geometric nonlinearity with updated-Lagrangian (McGuire et al. 2014) and co-rotational (Crisfield 1991) being two widely used approaches. For the standard *OpenSees* beam-column elements, the difference between geometric linear and geometric nonlinear analysis lies in the geometric transformation alone, since the elements have no internal geometric nonlinearity (Denavit and Hajjar 2013).

In the geometric transformation procedure, the global nodal displacements of the element are transformed to the natural (local) displacement by implementing the geometric transformation matrix (T). Element force and stiffness are calculated in *OpenSees* in the natural displacements. The transformation may be expressed as follows:

$$Q_G = T^T Q_N \quad (1)$$

where Q_G and Q_N are forces in the global and natural coordinate system, respectively and T is the transformation matrix. Three different types of geometric transformation are possible in *OpenSees*: Linear, Corotational and PDelta. In the Linear “transformation” the angles between the elements and coordinate system and also the length of the elements remains their initial values and will not change during the analysis – i.e. classical linear analysis. For the Corotational geometric transformation the values for all angles and lengths are estimates of the current position rather than the initial. In the PDelta transformation the difference between transverse displacements at the nodes in local coordinate are considered to implement the effects of second-order lateral translation of the member. As implemented in *OpenSees* the Corotational transformation should be the most accurate, but also the most numerically costly. The PDelta transformation should capture buckling and basic geometric nonlinearity but may have accumulated error in large deflections. Denavit and Hajjar (2013) provide some basic studies of the *OpenSees* geometric nonlinearity implementations. The intent here is to study the influence of these transformations in the context of larger 3D buildings and in time history response where inertial and damping effects may dominate over static geometric transformations.

4. Analysis Results

Models of the developed CBF and BRB steel-framed archetype buildings were used to conduct modal analysis, static pushover analysis, and nonlinear time history analysis. Of the developed archetypes the one-story CBF and four-story BRB are highlighted here. The impact of geometric nonlinearity on the response, as implemented in OpenSees, is examined herein.

4.1 One-story Archetype Building with CBF

The one-story CBF archetype is introduced in Section 2. The key nonlinearities in the model are the in-plane shear response of the bare steel deck roof and the response of the hollow structural section braces. The first mode period from the design model for the one-story CBF archetype building is 0.36 s.

4.1.1 CBF Nonlinear Static Pushover Analysis

Pushover analysis was conducted to study the static behavior of the archetype building. A displacement-controlled load pattern was applied to the structure in the short direction (long diaphragm span direction). Per FEMA P695, vertical distribution of the lateral force at each node was assigned proportional to the product of the tributary mass and the fundamental mode shape coordinate at the node obtained from eigenvalue analysis in *OpenSees*. Fig. 6 shows the applied load versus the story drift for increasing values of drift ratios and the magnified displaced shape in the post-peak regime for three different types of geometric transformations.

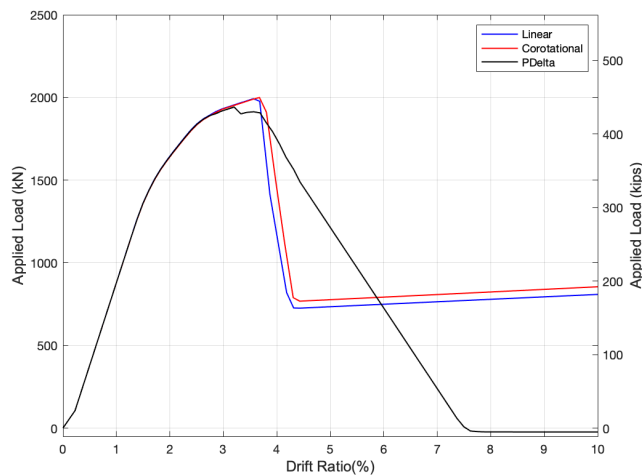


Figure 6: Pushover response of one-story CBF archetype building

Fig. 7 provides the displaced shape of the building at 80% post-peak response for two of the geometric transformations. The peak strength is in-sensitive to the selected geometric transformation, but the post-peak response depends strongly on the selected transformation method. As Fig. 7 shows the nonlinear diaphragm response is dominating the failure mode in the pushover analysis so the p-delta demands on the gravity columns are important to characterizing the failure. It is surprising that the PDelta and Corotational transformations are not in better agreement in this problem – and this observation is worthy of further study. It is possible that given the loss of in-plane diaphragm stiffness there is extra sensitivity to out-of-plane modeling assumptions and this is impacting the accuracy of the transformations, but at this point the true cause of the differences is unknown.

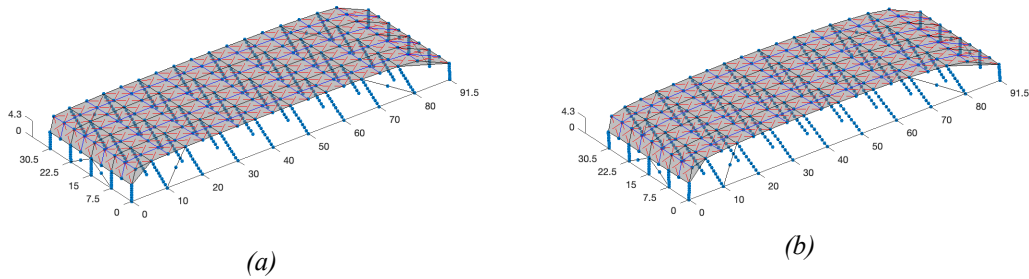


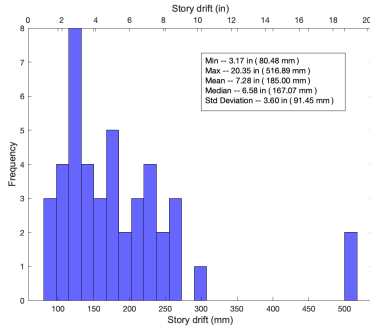
Figure 7: post-peak displaced shape for (a) Linear T (b) PDelta T

4.1.2 CBF Time History Response Analysis

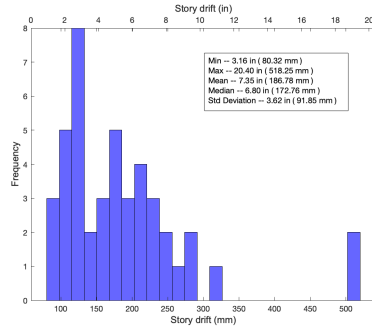
To evaluate the seismic performance of the archetype building and diaphragm system, nonlinear response time history analysis was performed with the building model subjected to the FEMA P695 suite of far-field earthquake motions. Two scale levels are considered for the nonlinear response history analysis: 1) Design Basis Earthquake (DBE) and 2) Maximum Considered Earthquake (MCE). The 44 ground motions are scaled accordingly to each desired level and are applied in the weak direction of the building. For DBE and MCE, the ground motions are scaled such that the median spectrum matches the design spectrum at the fundamental period of the building. Based on the procedures, the scale factors for the two levels considered are 1.05 and 1.58, respectively.

The predicted peak diaphragm drift across the studied earthquakes for the three studied geometric transformations is provided in Fig. 8. While individual results vary, the aggregated statistical results indicate relatively small differences. The PDelta and Corotational transformations, both of which capture geometric nonlinearity to differing degrees, are essentially the same. Even the Linear transformation, which ignores geometric nonlinearity, is close to the other time history results at DBE level and surprisingly does not provide particularly poor results even at MCE level. One could reasonably conclude from this small study that the inertial and damping effects are more important in this case than second-order (geometric nonlinear) effects. Note, the models include strong nonlinearity even in the Linear transformation case here since the nonlinear diaphragm and brace models are included, for all transformations.

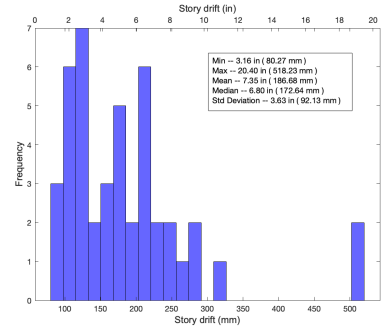
To examine the results in detail the median earthquake record response is also determined: at the DBE level this is Earthquake 8 (1999 Hector Mine) in the P695 suite and at the MCE level this is Earthquake 34 (1987 Superstition Hills) in the P695 suite. The time history of the drift response is provided in Fig. 9. The response is observed to generally be independent of the selected geometric transformation.



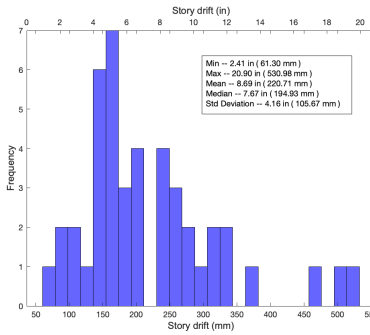
(a) DBE level- Linear T



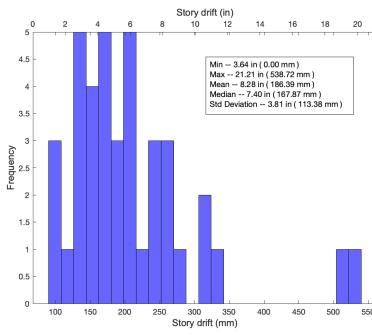
(b) DBE level- Corotational T



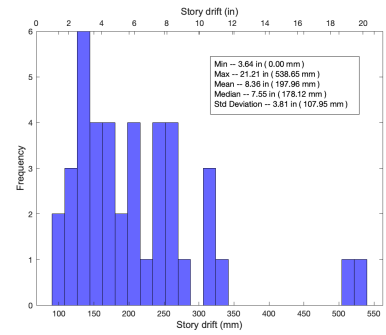
(c) DBE level- PDelta T



(d) MCE level- Linear T

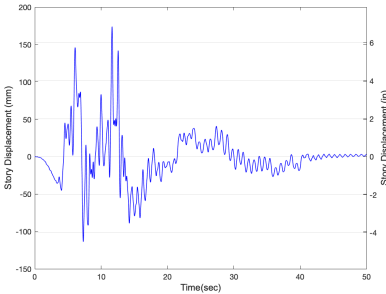


(e) MCE level- Corotational T

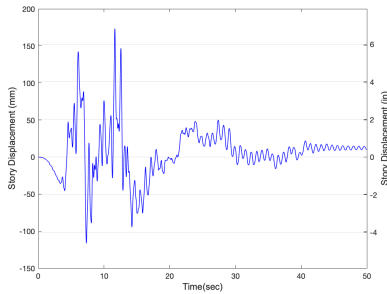


(f) MCE level- PDelta T

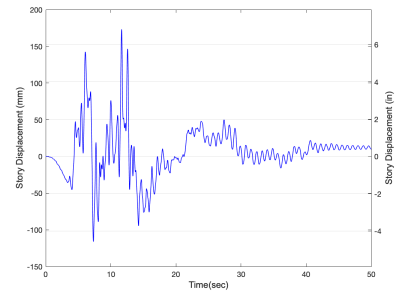
Figure 8: Diaphragm drift for three geometric nonlinearities



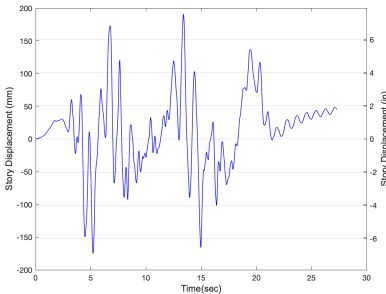
(a) DBE level- Linear T



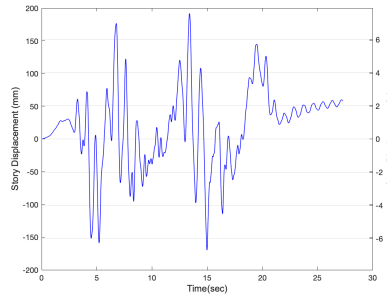
(b) DBE level- Corotational T



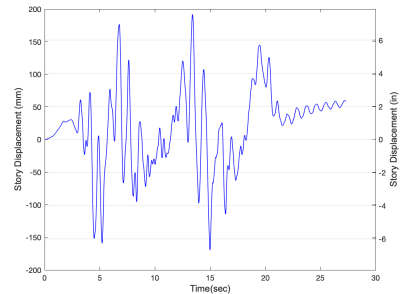
(c) DBE level- PDelta T



(d) MCE level- Linear T



(e) MCE level- Corotational T



(f) MCE level- PDelta T

Figure 9: Median EQ diaphragm drift at DBE and MCE level

Fig. 10 provides the distribution of the diaphragm shear strain and the displaced shape of the model (top down) at the peak diaphragm drift from the median DBE and MCE-level earthquakes. The results show that the peak roof shear strain in the diaphragm is less than 0.5% and 1.0% for DBE and MCE-level earthquakes, respectively. This may be compared with cyclically tested bare steel deck which has a peak shear strain of approximately 2% (O'Brien et al. 2017), indicating the median roof is not in a heavily damaged state in this model. Moreover, the results show similar response for shear strain and deformed shape for all three types of geometric transformations.

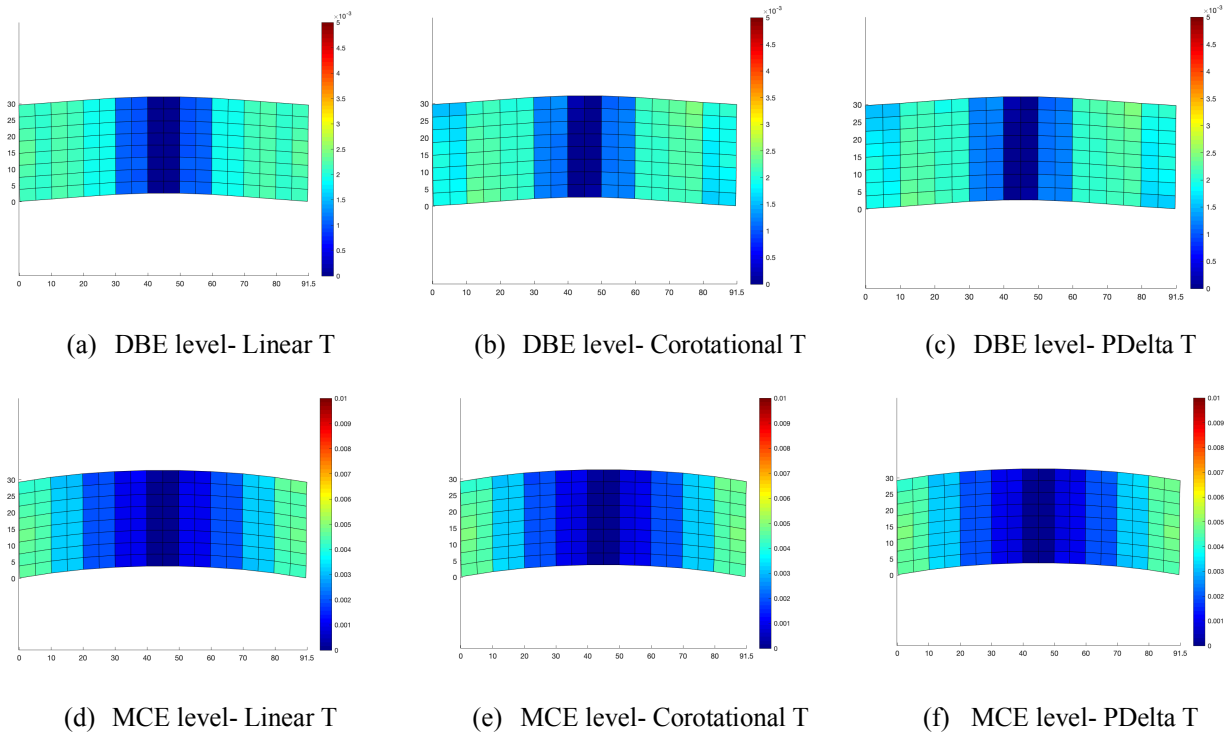


Figure 10: Shear strain of median BDE and MCE scaled earthquake at peak diaphragm drift

Fig. 11 provides the axial force distribution in the perimeter beams (chords on the long side, collectors on the short side) of the archetype building at the time of peak diaphragm drift for the median MCE-level earthquake and three different types of geometric transformation. As expected, the beams in the longer direction of the building are in tension in one side (red color) and in compression on the other side of the building (blue color). The distribution is influenced by the location of the braced bays, with larger axial forces in the braced bay to equilibrate the brace itself. The collector beams on the short side of the building have minimal axial force at the corners and maximum in the center, with the force in the beams dominated by the braces as opposed to the roof shear. It is in these results that we see for the first time a significant impact of the selected geometric transformation. The Linear transformation results in predicted chord forces that are only 2/3 that of the Corotational or PDelta transformation. It is perhaps surprising that these forces do not themselves results in large differences in drift for the different methods, as would be the case in a static analysis, but this only highlights the important impact of the inertial effects on drift in these dynamic analyses.

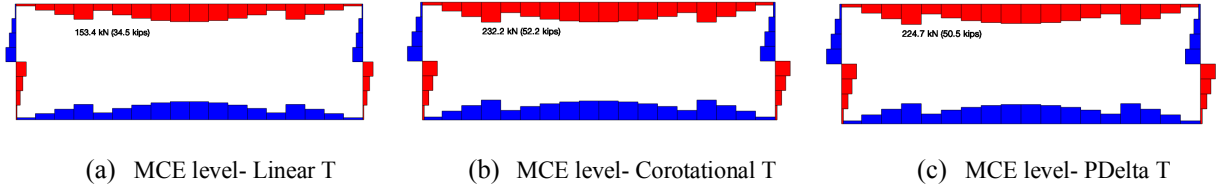


Figure 11: Axial force distribution in the perimeter beams of the archetype CBF building median MCE earthquake at peak drift

4.2 Four-story Archetype Building with BRB

The four-story BRB archetype is introduced in Section 2. The key nonlinearities in the model are the in-plane shear response of the concrete-filled deck floor diaphragms and the bare steel deck roof diaphragm and the response of the BRB braces. The first mode period from the design model for the four-story BRB archetype building is 1.13 s. The pushover response of this model is examined in detail here. Fig. 12 provides the overall drift response and the post-peak deformed shape of the building for the Corotational geometric transformation.

The pushover response of the four-story BRB, across the analysis types, is more aligned with expectations. The BRB yields, and the P-delta effect on the gravity columns is crucial to accurately developing the response. The Linear transformation ignores this influence, and predicts that the yielding of the BRBs equates to the strength of the building. The geometric nonlinear transformations capture accurately that the BRB yielding results in large second-order effects in the frames that create an overall negative post-peak response despite the positive strain hardening of the BRB itself (Fig. 4b)

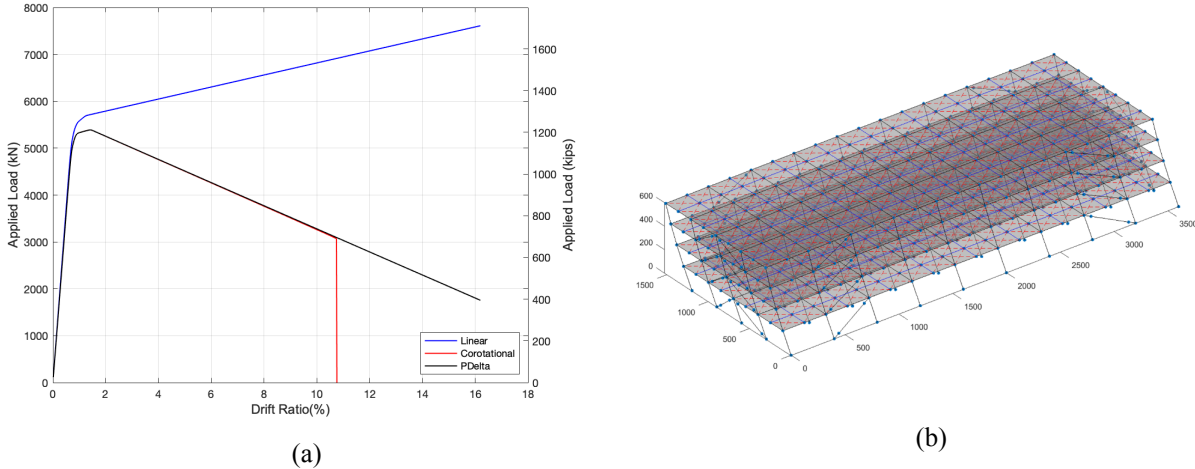


Figure 12: Pushover response of archetype building (a) force-displacement (b) post-peak displaced shape for corotational T

To illustrate this important P- Δ effect on the four-story archetype building, the equilibrium of the building is studied for the approximate deformed shape of the building with an incremental displacement $d\Delta$ at the top and the resulting lateral force decrement $dV_{P-\Delta}$ due to P- Δ effect. Fig. 13 provides the idealized deformed shape and loading for the building which is assumed as a rigid body with the displacement at each level Δ_i and its increment $d\Delta_i$ proportional to the height of the level, h_i .

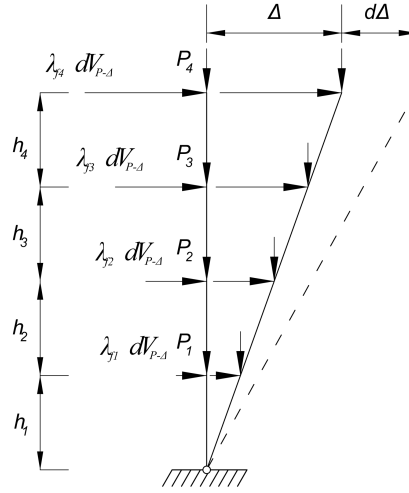


Figure 13. Deformed shape and loading for P- Δ effect

Eq. 2 provides the moment equilibrium for the four-story archetype building.

$$\sum_{i=1}^4 (\lambda_{fi} dV_{p-\Delta} h_i + p_i d\Delta_i) = 0 \quad (2)$$

Where p_i is the gravity load, λ_{fi} is the load pattern (ratio of the lateral load applied on each level to the total applied lateral load) and $d\Delta_i$ can be approximated as

$$d\Delta_i = \frac{h_i}{H} d\Delta \quad (3)$$

In Eq. 3, H is the total height of the building. The approximate slope of the strength degradation with increasing displacement due to P- Δ effect can be introduced as:

$$\frac{d\Delta_{P-\Delta}}{d\Delta} = - \frac{\sum_{i=1}^4 p_i \frac{h_i}{H}}{\sum_{i=1}^4 \lambda_{fi} h_i} \quad (3)$$

In the pushover analysis, strain hardening of the BRBs should also be considered for the degrading segment of the pushover curve, which can be obtained by the pushover analysis without including the P- Δ effect (see Fig. 12). Table 4 shows the results from the calculations and the analysis. The approximated degrading slope from the calculation is -14.02 kN/mm (8.01 kip/in), and the degrading slope from the analysis is -15.91 kN/mm (-9.09 kip/in). This discrepancy can be explained by the fact that the deformation along the building height is not linear, with the actual deformations at most of the stories from the analysis larger than the assumed ones in the calculation, and that the diaphragms deformations also contribute to a larger P- Δ effect (see Fig. 12).

Table 4: P-Δ effect and strength degradation for four-story BRB archetype building

| Level | h_x (mm) | P_x (kN) | λ_{fx} | $P_x \cdot \frac{h_x}{\sum h_x}$ (kN) | $\lambda_{fx} \cdot h_x$ (mm) | $\frac{dV_{P-\Delta}}{d\Delta}$ (kN/mm) | $\left(\frac{dV}{d\Delta}\right)_{hardening}^{BRB}$ (kN/mm) | $\left(\frac{dV}{d\Delta}\right)_{calc}$ (kN/mm) | $\left(\frac{dV}{d\Delta}\right)_{analysis}$ (kN/mm) |
|-------|-------------------|----------------------|----------------|--|----------------------------------|--|--|---|---|
| Roof | 15697 (618 in) | 6605 (1485 kips) | 0.345 | 660.6 (148.5 kips) | 5412.7 (213.1 in) | | | | |
| 3 | 11887 (468 in) | 12504 (2811 kips) | 0.352 | 947.0 (212.9 kips) | 4183.4 (164.7 in) | -22.21 (-12.69 kip/in) | 8.19 (4.68 kip/in) | -14.02 (-8.01 kip/in) | -15.91 (-9.09 kip/in) |
| 2 | 8077 (318 in) | 12504 (2811 kips) | 0.205 | 643.2 (144.6 kips) | 1657.4 (65.2 in) | | | | |
| 1 | 4267 (168 in) | 12615 (2836 kips) | 0.098 | 343 (77.10 kips) | 418.6 (16.5 in) | | | | |
| | | | Σ | 2593.8 (583.1 kips) | 11671.6 (459.5 in) | | | | |

5. Discussion

Significant work remains to fully explore the seismic performance of 3D steel framed buildings. The work herein provides a reporting of in progress efforts to use building simulations to better understand the impact of changes to diaphragm design and the impact of modeling choices, particularly the inclusion of geometric nonlinearity. Work underway is considering 1, 4, 8, and 12 story building examples for both the BRB and CBF frames. It is anticipated that with this larger study more definitive conclusions can eventually be reached. The four-story BRB example unequivocally demonstrates the importance of geometric nonlinearity in static analyses; however, the available time history analyses are not as conclusive. Other sources of nonlinearity in a building response may be more important than the application of geometric nonlinearity for the overall model - significant work remains.

6. Conclusions

The seismic performance of steel braced frames depends on the nonlinear performance of both the vertical and horizontal lateral force resisting systems and the predicted behavior may be sensitive to basic assumptions included in analysis. As design specifications evolve new questions arise. What is the impact of new diaphragm design provisions implemented in ASCE 7? What is the impact of ignoring geometric nonlinearity in seismic design? Using a series of archetype building designs the work reported herein attempts to begin to address these questions. Three-dimensional OpenSees models of a one-story CBF and four-story BRB building are explored. The models include nonlinearity in the braced frames, as well as in the in-plane diaphragm response. The impact of geometric nonlinearity can be complex in the building response. A one-story CBF pushover example is shown where the diaphragm nonlinearity governs and the response is not overly sensitive to geometric nonlinearity, while in a four-story BRB pushover example the vertical system yields and the degrading slope can be directly attributed to the increasing P-delta (geometric nonlinear) demands. In dynamic analysis, geometric nonlinear effects compete with inertial and damping effects and the one-story CBF example demonstrates that building drift may not be overly sensitive to geometric nonlinearity, but internal forces are sensitive. Much work remains to expand the current studies and reach definitive conclusions on the selected research questions.

Acknowledgments

This work was supported by the National Science Foundation under Grant No. 1562669 and the Steel Diaphragm Innovation Initiative which is funded by AISC, AISI, SDI, SJI, and MBMA. Any opinions expressed in this paper are those of the authors alone, and do not necessarily reflect the views of the National Science Foundation or other sponsors.

References

- American Society of Civil Engineers. (2010). "Minimum design loads for buildings and other structures (ASCE standard)", Reston, Va. *American Society of Civil Engineers*.
- Crisfield, M. (1991). "Nonlinear Finite Element Analysis of Solids and Structures: Volume 1: Essentials." *John Wiley & Sons*.
- Denavit, D. M., Hajjar, F.J., (2013). "Description of geometric nonlinearity for beamcolumn analysis in OpenSees", Report NEU-CEE-2013-02, *Department of Civil and Environmental Engineering, Northeastern University, Boston, Massachusetts*. <http://hdl.handle.net/2047/d20003280>.
- Eatherton, M. R., Fahnestock, L. A., Miller, D. J. (2014). "Computational study of self-centering buckling-restrained braced frame seismic performance." *Earthquake Engineering & Structural Dynamics*, 43(13) 1897-1914.
- EERI (1996). "Northridge Earthquake Reconnaissance Report, Vol. 2 Earthquake Spectra - Supplement C to Volume 11" *Earthquake Engineering Research Institute*.
- Fahnestock, L. A., Ricles, J. M., & Sause, R. (2007). "Experimental evaluation of a large-scale buckling-restrained braced frame." *Journal of structural engineering*, 133(9) 1205-1214.
- Fell, B.V., Kanvinde, A.M., Deierlein, G.G., Myers, A.T. (2009). "Experimental investigation of inelastic cyclic buckling and fracture of steel braces." *Journal of structural engineering*, 135(1) 19-32.
- Fillipou, F. C., Popov, E. P., Bertero, V. V. (1983). "Effect of bond deterioration on hysteretic behaviour of reinforced concrete joints." Report EERC 83-19, *Earthquake Engineering Research Center, University of California, Berkeley, CA*.
- Han, S.W., Kim, W.T., Foutch, D.A. (2007). "Seismic behavior of HSS bracing members according to width-thickness ratio under symmetric cyclic loading." *Journal of Structural Engineering*, 133(2) 264-273.
- Lowes, L. N., Altoontash, A. (2003). "Modeling reinforced-concrete beam-column joints subjected to cyclic loading." *Journal of Structural Engineering*, 129(12) 1686-1697.
- Martin, É. (2002). "Inelastic response of steel roof deck diaphragms under simulated dynamically applied seismic loading." Master's thesis, *Ecole Polytechnique de Montreal*.
- McGuire, W. Gallagher, R.H., Ziemian, R. (2014). "Matrix Structural Analysis, 2nd Ed." *John Wiley & Sons*.
- O'Brien, P., Eatherton, M. R., & Easterling, W. S. (2017). "Characterizing the load-deformation behavior of steel deck diaphragms using past test data." CFSRC Report, <https://jscholarship.library.jhu.edu/handle/1774.2/40633>
- Popov, E. P., Black, R. G. (1981). "Steel struts under severe cyclic loadings." *Journal of the Structural Division*, 107(9) 1857-1881.
- Qayyum, B. (2017). "Computational modeling of one-story buildings with nonlinear steel deck diaphragms subjected to earthquakes." Report, *Virginia Tech*.
- Rodriguez, M., Restrepo, J., Blandón, J. (2007). "Seismic design forces for rigid floor diaphragms in precast concrete building structures". *Journal of Structural Engineering*, 133(11) 1604-1615.
- Torabian, S., Eatherton, M.R., Easterling, W.S., Hajjar, J.F., Schafer, B.W. (2017) "SDII Building Archetype Design v1.0" CFSRC Report R-2017-04, <https://jscholarship.library.jhu.edu/handle/1774.2/40638>.